Exploration of the subcycle multiphoton ionization dynamics and transient electron density structures with Bohmian trajectories

Hossein Z. Jooya, Dmitry A. Telnov, Peng-Cheng Li, and Shih-I Chu

Phys. Rev. A **91**, 063412 — Published 18 June 2015

DOI: 10.1103/PhysRevA.91.063412

Exploration of the sub-cycle multiphoton ionization dynamics and transient electron density structures with Bohmian trajectories

Hossein Z. Jooya[1,*], Dmitry A. Telnov[2], Peng-Cheng Li[3,4], and Shih-I Chu[1,3,*]

[1] *Department of Chemistry, University of Kansas, Lawrence, Kansas 66045, USA*
[2] *Department of Physics, St. Petersburg State University, St.Petersburg 198504, Russia*
[3] *Center for Quantum Science and Engineering, Department of Physics, National Taiwan University, Taipei 10617, Taiwan*
[4] *College of Physics and Electronic Engineering, Northwest Normal University, Lanzhou, Gansu 730070, China*

* jooya@ku.edu , sichu@ku.edu

PACS numbers: 32.80.Rm,42.50.Hz

Abstract

An accurate 3D numerical scheme for the De Broglie–Bohm's framework of Bohmian mechanics is presented. This method is utilized to explore the sub-cycle multiphoton ionization dynamics of the hydrogen atom subject to intense near infrared (NIR) laser fields on the sub-femtosecond time scale. The analysis of the time-dependent electron density reveals that several distinct density portions can be shaped and detached from the core within a half cycle of the laser field. As a complementary perspective, we identify several distinct groups of the Bohmian trajectories which represent the multiple detachments of the electron density at different times. The method presented provides very accurate electron densities and Bohmian trajectories that allow to uncover the origin of the formation of the transient and distinct electron structures seen in the MPI processes.

The recent development of attosecond metrology has enabled the real-time experimental observation of ultrafast electron dynamics in atomic and molecular systems [1,2]. Considerable interest has been recently paid also to the study of transient absorption spectroscopy in ultrafast time domain [3-5]. For example, the observation of the transient changes in the absorption of an isolated attosecond XUV pulse by helium atoms in the presence of a delayed few-cycle NIR laser pulse has been recently reported and uncovered novel absorption structures corresponding to laser-induced "virtual" intermediate states in the two-color two-photon (XUV + NIR) and three photon (XUV+ NIR + NIR) absorption processes [5]. These previously unobserved absorption structures are modulated on half-cycle (~ 1.3 fs) and quarter-cycle (~ 0.6 fs) time scales, resulting from quantum optical interference in the laser-driven atom. More recently, there is also new interest in the study of sub-cycle transient high harmonic generation (HHG) dynamics and ultrafast spectroscopy in the attosecond time domain [6,7] as well as the sub-cycle transient structures in time-dependent multiphoton ionization (MPI) processes [8,9]. These recent studies have revealed novel transient multiphoton dynamics and spectroscopy in the ultrashort time domain. In this paper, we focus on the exploration of the transient MPI dynamics and we uncover the origin of the generation of the transient and distinct electron density structures seen in the MPI processes for the first time by means of the Bohmian quantum trajectory approach.

In the study of strong-field HHG and MPI processes, the classical and semi-classical trajectory methods have been widely used in the past and they are valuable in providing qualitative insight regarding the multiphoton dynamics. For the HHG processes, the 3-step model [10,11] and strong-field approximation (SFA) [12] are often used. However, the SFA does not take into account the Coulomb potential and electronic structure and cannot be used for the study of below- and near- threshold multiphoton processes, for example. Fully *ab initio* quantum mechanical solution of the time-dependent Schrödinger equation (TDSE) is currently feasible for one- and two- electron systems for the accurate treatment of MPI and HHG processes Bohmian mechanics (BM) [13] is an alternative and complementary quantum approach which can provide a trajectory-based scheme allowing for a causal interpretation of quantum mechanics. Information on individual trajectories, along with the analysis of the emission times of various groups of trajectories prepares a comprehensive and intuitive picture of the process under investigation. Therefore, this method can serve in complement to the results obtained from direct analysis of the electron density. The BM approach has been successfully applied to the model study of problems such as photo-dissociation [14], tunneling [15], and atom diffraction by surface [16], etc., in the past. More recently, it has been also used to the model study of strong field processes such as HHG [17], laser-driven electron dynamics [18-25], etc.

However, most of the BM studies of strong field processes so far have adopted either 1D or soft-potential models. In this article, we present a fully *ab initio* 3D and accurate treatment of the Bohmian trajectories beyond SFA, and discuss the formation of sub-cycle transient structures seen in the MPI processes.

We treat the interaction of an intense laser field with a single hydrogen atom by solving the time-dependent Schrödinger equation (TDSE) (atomic units are used):

$$i\frac{\partial}{\partial t}\psi(\boldsymbol{r},t)=\left[\hat{H}_0+\hat{V}(\boldsymbol{r},t)\right]\psi(\boldsymbol{r},t), \tag{1}$$

where $\hat{H}_0$ is the unperturbed Hamiltonian of the hydrogen atom and $\hat{V}(r,t)$ is the time-dependent interaction of the electron with the laser field in the dipole approximation:

$$\hat{V}(\boldsymbol{r},t)=-\boldsymbol{F}(t)\boldsymbol{r}=-zF(t), \tag{2}$$

$\boldsymbol{F}(t)$ being the force acting upon the electron from the laser field. For the sine-squared envelope of the laser pulse,

$$F(t) = F_0 sin^2(\frac{\pi t}{T}) sin(\omega t), \tag{3}$$

where F_0 is the peak field amplitude, ω is the carrier frequency, and T is a pulse duration. Without loss of generality, we can assume that the polarization vector of the field lies in *z*-direction. In all our calculations we have used a laser pulse with the sine-squared envelope, total duration of 20 optical cycles (o.c.), the carrier wavelength 800 nm (corresponding to the photon energy 1.55 eV), and the peak intensity $8\times10^{13} W/cm^2$.

The time-dependent generalized pseudo-spectral (TDGPS) method [26] is used to solve the TDSE in spherical coordinates accurately and efficiently. This method takes advantage of the generalized pseudo-spectral (GPS) technique for non-uniform optimal spatial discretization of the coordinates and the Hamiltonian using only a modest number of grid points. The time propagation of the wave function under this method is performed by the split operator method in the energy representation [26]:

$$\begin{aligned} &\psi(r, t+\Delta t) \\ &\cong \exp\left(-i\hat{H}_0 \frac{\Delta t}{2}\right) \times \exp\left[-iV\left(\boldsymbol{r}, \theta, t+\frac{\Delta t}{2}\right)\Delta t\right] \\ &\times \exp\left(-i\hat{H}_0 \frac{\Delta t}{2}\right) + O\left(\Delta t^3\right). \end{aligned} \tag{4}$$

To impose correct outgoing-wave boundary conditions on the wave function and prevent spurious
reflections from the boundary of the spatial domain, we use an absorbing layer at large distances from the atomic core. The absorber is implemented through the mask function $\cos^{0.25}[\pi(r-r_0)/2(r_{\max}-r_0)], (r \geq r_0)$ with $r_{\max} = 100 a.u.$, $r_0 = 80 a.u.$. The wave function is multiplied by the mask function at each time step. Because of the absorber, the norm of the wave function decreases in time. The time-dependent ionization rate can be defined as a logarithmic derivative of the time-dependent population $P(t)$ [8]:

$$P(t) = \int \left|\psi(\boldsymbol{r}, t)\right|^2 d^3 r, \tag{5}$$

$$\Gamma(t) = -\frac{d}{dt} ln P(t). \tag{6}$$

For atoms in linearly polarized laser fields, the angular momentum projection onto the polarization direction of the field (the z-axis) is conserved. That means the dependence of the wave function on the angle φ (rotation angle about the z-axis) is reduced to the factor $\exp(im\varphi)$, where m is the angular momentum projection. For $m=0$ the wave function does not depend on φ at all, thus the gradient of the wave function ψ can be calculated with respect to the coordinates r (radial coordinate) and θ (angle between the radius-vector and z-axis):

$$\nabla \psi = \boldsymbol{e}_r \frac{\partial \psi}{\partial r} + \boldsymbol{e}_\theta \frac{1}{r}\frac{\partial \psi}{\partial \theta} = \boldsymbol{e}_r \frac{\partial \psi}{\partial r} - \boldsymbol{e}_\theta \frac{sin\theta}{r}\frac{\partial \psi}{\partial cos\theta} . \tag{7}$$

$\boldsymbol{e}_r$ and $\boldsymbol{e}_\theta$ are the unit vectors of spherical coordinate system. The equation for the Bohmian trajectories reads as

$$\frac{d\boldsymbol{r}}{dt} = Im\frac{\nabla \psi}{\psi} , \tag{8}$$

We note that our approach is fully based on quantum mechanics. The right-hand side of Eq.(8) represents the velocity field from an accurate quantum-mechanical wave function. Thus there is no discrepancy between the analysis based on quantum-mechanical fluxes and that based on the Bohmian trajectories. Since the velocity $\frac{d\boldsymbol{r}}{dt}$ has the following expansion in the spherical coordinate system,

$$\frac{d\boldsymbol{r}}{dt} = \boldsymbol{e}_r \frac{dr}{dt} + \boldsymbol{e}_\theta r\frac{d\theta}{dt} + \boldsymbol{e}_\varphi r sin\theta \frac{d\varphi}{dt}, \tag{9}$$

the vector equation (8) is equivalent to a set of three 1D equations:

$$\frac{dr}{dt} = Im\left(\frac{1}{\psi}\frac{\partial \psi}{\partial r}\right), \tag{10}$$

$$\frac{d\theta}{dt} = -\frac{sin\theta}{r^2} Im\left(\frac{1}{\psi}\frac{\partial \psi}{\partial cos\theta}\right), \tag{11}$$

$$\frac{d\varphi}{dt} = 0 . \tag{12}$$

Obviously, the angle φ does not change, and the trajectory lies in the plane defined by the initial (at $t = t_0$) radius-vector and the z-axis. One has to solve the Cauchy problem for the set of two equations (10) and (11). In the generalized pseudo-spectral (GPS) discretization, we use the Gauss-Lobatto scheme for the variable r (with the appropriate mapping transformation) and the

Gauss scheme for the variable $cos\theta$. The expression for the first derivative with respect to r appears as following:

$$\left(\frac{\partial\psi}{\partial r}\right)_{r(x_i)} = \frac{1}{r'(x_j)}\sum_{j'=1}^{N_x}\frac{P_{N_x+1}(x_j)}{P_{N_x+1}(x_{j'})} d_{jj'}^{x}\psi\left((x_{j'})\right), \tag{13}$$

Here, P_{N_x+1} is the Legendre polynomial. N_x is the number of collocation points (roots of the derivative of Legendre polynomial, $P'_{N_x+1}(x)$), not including the end points -1 and +1. The matrix elements for the $d_{jj'}^{x}$ Gauss-Lobatto discretization are as listed below [27]:

$$d_{jj'}^{x} = \frac{1}{x_{j'} - x_j}\ (j \neq j'), \quad d_{jj}^{x} = 0\ (j \neq 0, j \neq N)$$

$$d_{00}^{x} = -\frac{N(N+1)}{4}\ ,\ d_{NN}^{x} = \frac{N(N+1)}{4}, \tag{14}$$

The first derivative with respect to $cos\theta$ is as follows:

$$\left(\frac{\partial\psi}{\partial cos\theta}\right)_{cos\theta_j} = \sum_{j'=1}^{N_y}\frac{P'_{N_y}(y_j)}{P'_{N_y}(y_{j'})} d_{jj'}^{y}\psi\left((cos\theta_{j'})\right) \tag{15}$$

Here N_y is the number of collocation points in the Gauss scheme (roots of the Legendre polynomial P_{N_y}). Eq.(15) assumes that the mapping transformation is just the identity transformation, i.e. $cos\theta = y$. The matrix elements $d_{jj'}{}^{y}$ are defined as following [28]:

$$d_{jj'}^{y} = \frac{1}{y_j - y_{j'}}\ (j \neq j'), \quad d_{jj}^{y} = \frac{y_j}{1 - y_j^2}, \tag{16}$$

To calculate the first derivative of the Legendre polynomials, one can use the following recursion relation:

$$P_{N_y}^{'}(y) = \frac{N_y(N_y+1)}{(2N_y+1)(1-y^2)}\left[P_{N_y-1}(y) - P_{N_y+1}(y)\right]. \tag{17}$$

The set of coupled ordinary differential equations (10) and (11) is solved numerically with the help of the 4th order Runge-Kutta (RK4) method, yielding the electron quantum trajectories. Since the quadrature points for RK4 differ from the original GPS grid points, we need to perform an additional interpolation using the GPS interpolation formula [29], to be able to evaluate the numerical values of the wave function at the coordinate points supplied by the RK4 solver:

$$\psi(r,\theta,t)=\sum_{i=1}^{N_x}\sum_{j=1}^{N_y}\psi(r_i,\theta_j,t)\frac{P_{N_x+2}(x)-P_{N_x}(x)}{(2N_x+3)(x-x_i)P_{N_x+1}(x_i)}\times$$

$$\frac{(2N_y+1)(1-y_j^{\,2})P_{N_y}(y)}{N_y(N_y+1)(y-y_j)\left[P_{N_y-1}(y_j)-P_{N_y+1}(y_j)\right]}. \tag{18}$$

In Fig.1, we use Bohmian trajectories to illustrate the dynamics of electron and its ionization rate within 7 optical cycles (5th-11th) of the given laser field, Fig.1(a). From left to right in Fig.1(b) one can see how distinct groups of Bohmian trajectories eventually are being formed at higher optical cycles. During the 5th optical cycle (the left most panel, shaded in green in Fig.1(b)) only one group of trajectories is distinguishable. As will be discussed later, these trajectories are representing a single portion of electron density detached from the core toward negative z-direction. When the laser electric field changes sign, some portion of these trajectories change direction and travel back to the core. The retuning process happens in a time interval of about 0.5 o.c. Since the returning trajectories travel different distances before they change direction and return to the core, each of them would have different return energies. This causes transitions to excited bound and continuum states of the unperturbed atom over time, resulting in the oscillations of the electron density. Therefore when the next ionization is about to happen toward negative z-direction, these oscillations of the electron density give rise to multiple wave packets, instead of just one. As can be seen in Fig.1(b) this effect becomes more and more influential at higher optical cycles up to the maximum laser intensity (11th optical cycle). By symmetry, the similar behavior happens for the trajectories travelling toward positive z-direction within the second half of each optical cycle. This effect is clearly pronounced as multiple bursts in the MPI rate diagram, Fig.1(c). We will discuss this in more detail later on in this article.

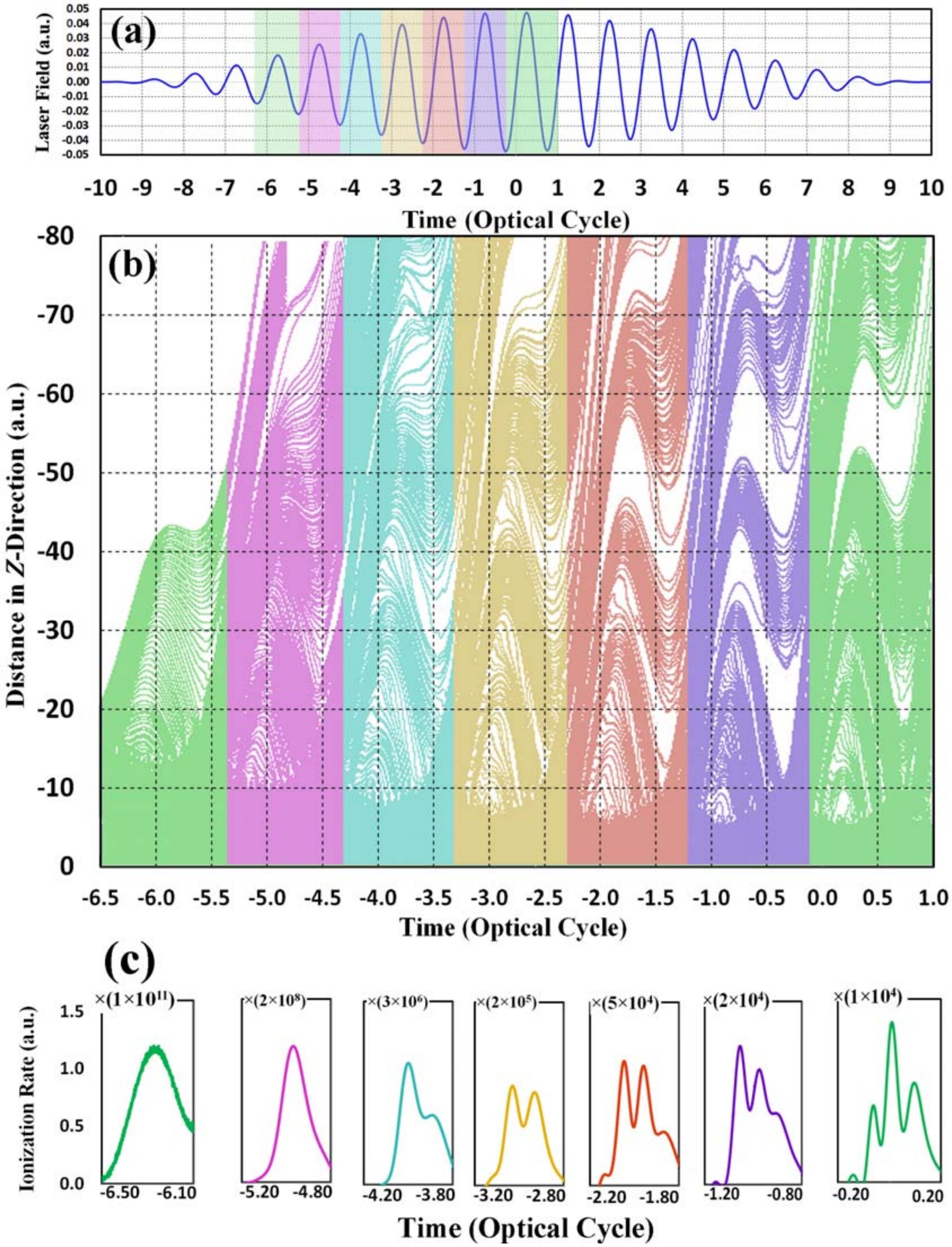

FIG.1. (Color online) (a) The 800 nm sin^2 driving laser pulse with the peak intensity of $8\times10^{13} W/cm^2$. Shaded in different colors, are the regions where Bohmian trajectory calculations are performed. (b) Bohmian trajectories computed within the time intervals given in (a). (c) Corresponding ionization rate plots within first-half optical cycle of the investigated time intervals. Distinct groups of electron trajectories eventually form from left to right, which in turn cause multiple bursts in ionization rate.

A detailed picture of the electron dynamics during the ionization process can be achieved by combining an analysis of the Bohmian trajectories and that of the time evolution of the electron density. In Fig.2, the evolution of the electron density of hydrogen atom is presented within the 11^{th} o.c. of the laser field. As illustrated in this figure, several distinct density portions are shaped and detached from the atom within a half optical cycle of the laser field. These multiple detachments of electron density from the core happen at different times, not necessarily when the external field reaches its maximum value. The oscillations of the electron density are caused by transitions to excited bound and continuum states in the laser field [8]. Besides the portions of electron density that leave the core after direct ionization, some detached wave packets return to the parent ion when the force from the laser field becomes positive (after 0.25 o.c.). As illustrated by the red and green colors, some of these wave packets travel longer (L), and some have shorter travel time (S), respectively, before they can return to the core. Bohmian trajectories corresponding to each of these wave packets will be further analyzed below.

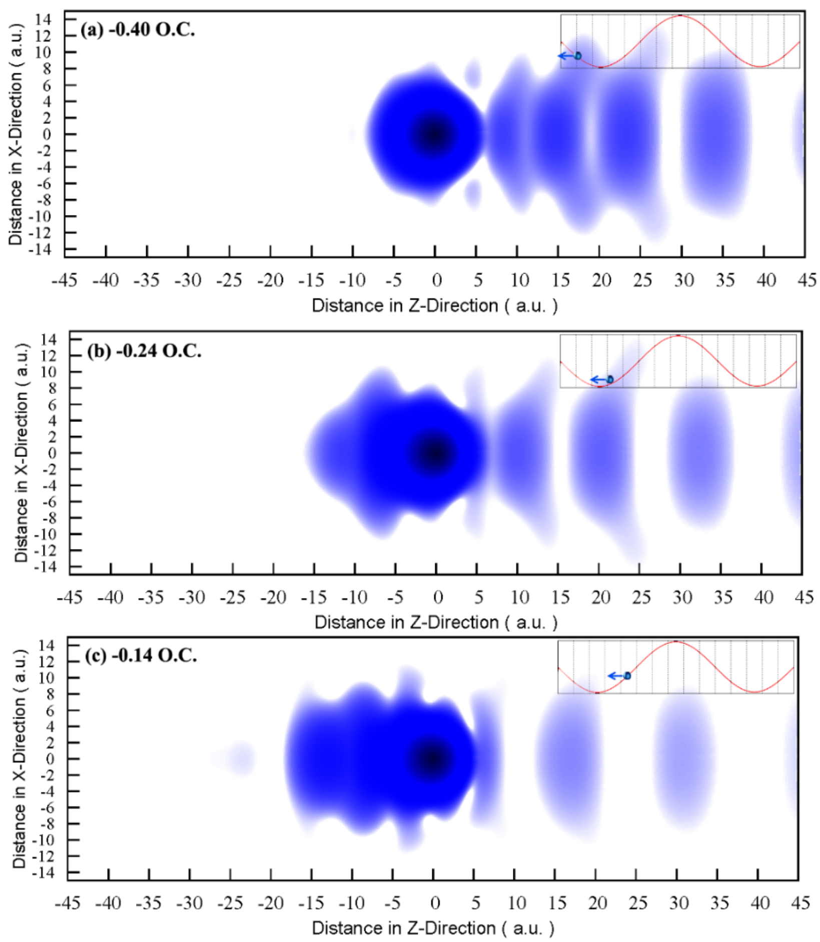

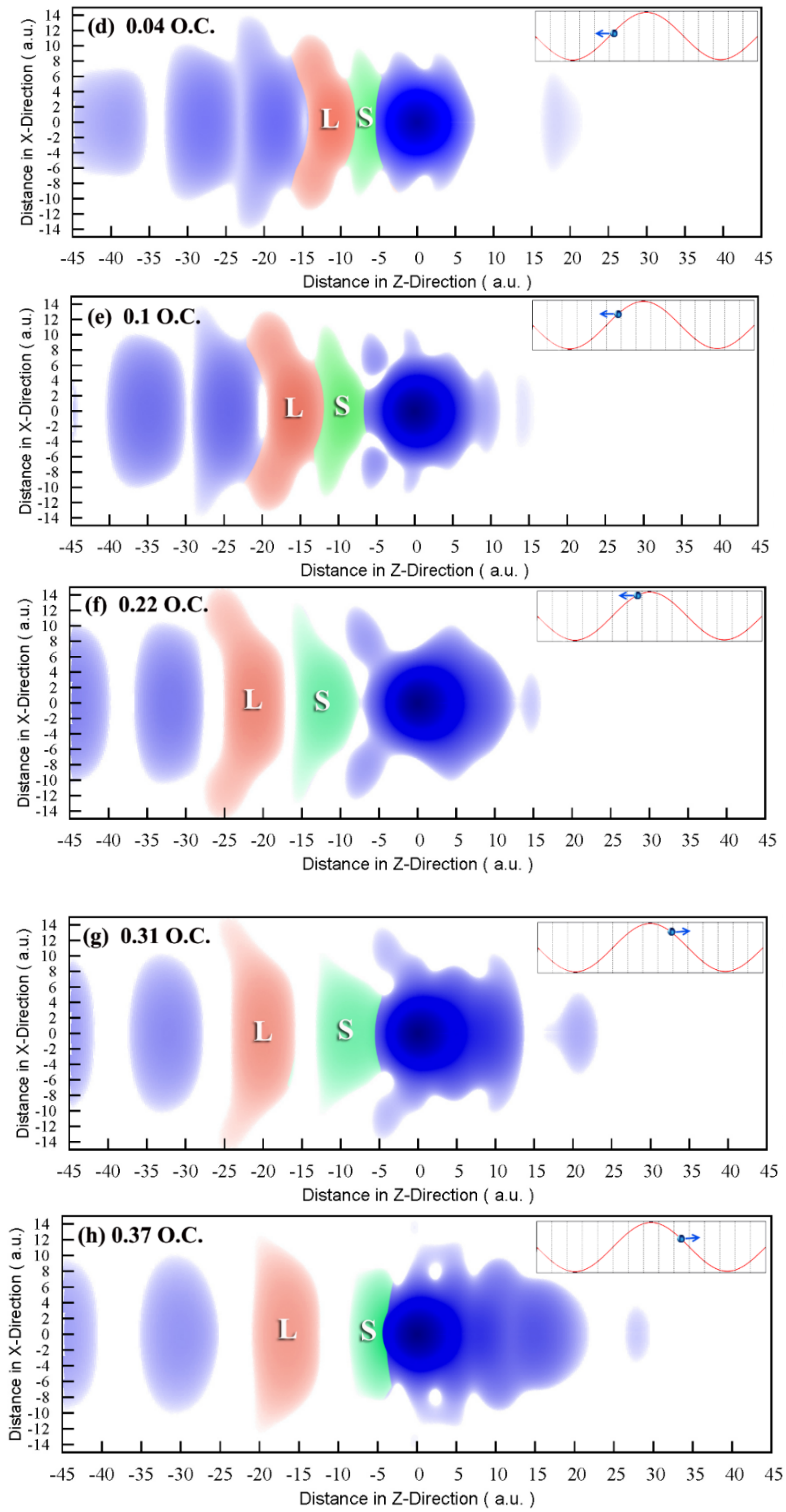
(d) 0.04 O.C.
(e) 0.1 O.C.
(f) 0.22 O.C.
(g) 0.31 O.C.
(h) 0.37 O.C.
L
S
Distance in X-Direction (a.u.)
Distance in Z-Direction (a.u.)

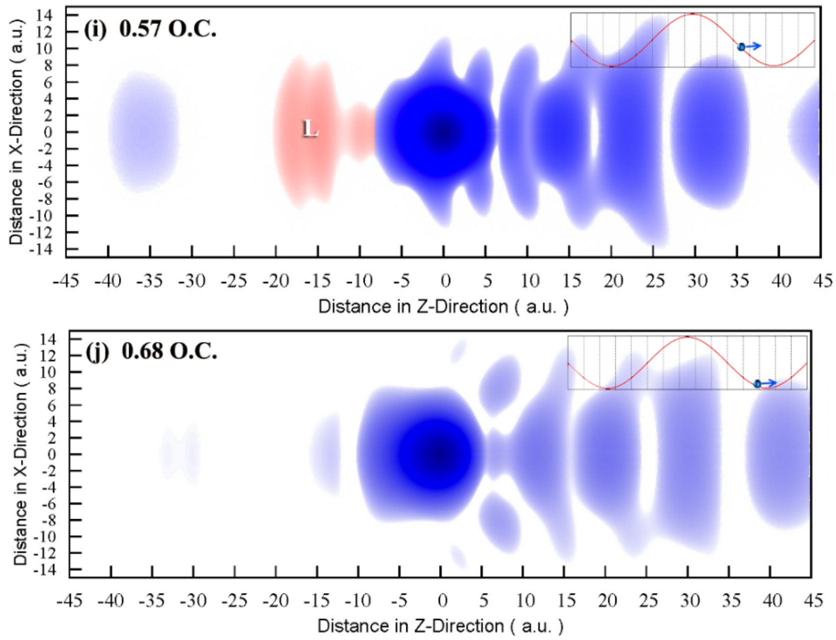

FIG.2. (Color online) Sub-cycle electron density evolution of the hydrogen atom in the 800 nm sin^2 laser pulse with the peak intensity of $8\times10^{13} W/cm^2$. Horizontal axis is the distance in the z-direction and the vertical axis shows the distance in the x-direction. The laser is polarized in the z-direction. The inset shows the corresponding phase of the laser field. The direction of the force from the laser field is illustrated by a small arrow. The laser field in the inset is shown for the interval -0.5 to +1.0 o.c. with the grid lines spacing of 0.1 o.c. The red and green regions represent the wavepackts returning to the core after a longer (L) and shorter (S) travel time, respectively. The color scale for the density is logarithmic.

In order to explore the dynamical mechanism of electron wave packet motion, we have performed semi-classical calculations, extending the standard approach suggested independently by Corkum [10] and Kulander et al. [11], with the inclusion of the Coulomb potential. Here, the electric force corresponding to the applied laser field is $\boldsymbol{F}_z = F(t)\boldsymbol{e}_z$, where $\boldsymbol{e}_z$ is the unit vector in the z-direction and *F(t)* is given by Eq. (3). When $\boldsymbol{F}_z$ and the electron velocity have the same direction, the electron gains the energy to escape the potential well. In Fig. 3(a), the result of the semi-classical approach is presented as electron return energy versus time. The initial conditions are set as $x_0 = y_0 = 17$ a.u, $z_0 = 0$, $v_{x0} = v_{y0} = 0, v_{z0} = -0.1$ a.u. The return energy is calculated as $E_k + E_p$, where E_k and E_p are the kinetic and Coulomb potential energies, respectively, when z coordinate of the electron returns to its initial value $z = 0.0 a.u.$. Here, we can indicate the short and long trajectories as those in the standard three-step model. As shown in this figure, the trajectories that are released late and return early are regarded as the short trajectories (green region), while those released early and returned late are the long trajectories (red region). The corresponding time intervals are shaded with the same colors in Fig. 3(b) on the laser field plot. Here the labels b through j correspond to the time moments for which the electron densities are presented in Fig. 2. The important feature of this result is the agreement between the ionization and return time periods predicted by semi-classical results and the one obtained from analyzing the electron density evolution and also determined by Bohmian trajectory calculations. The later result will be discussed in detail next.

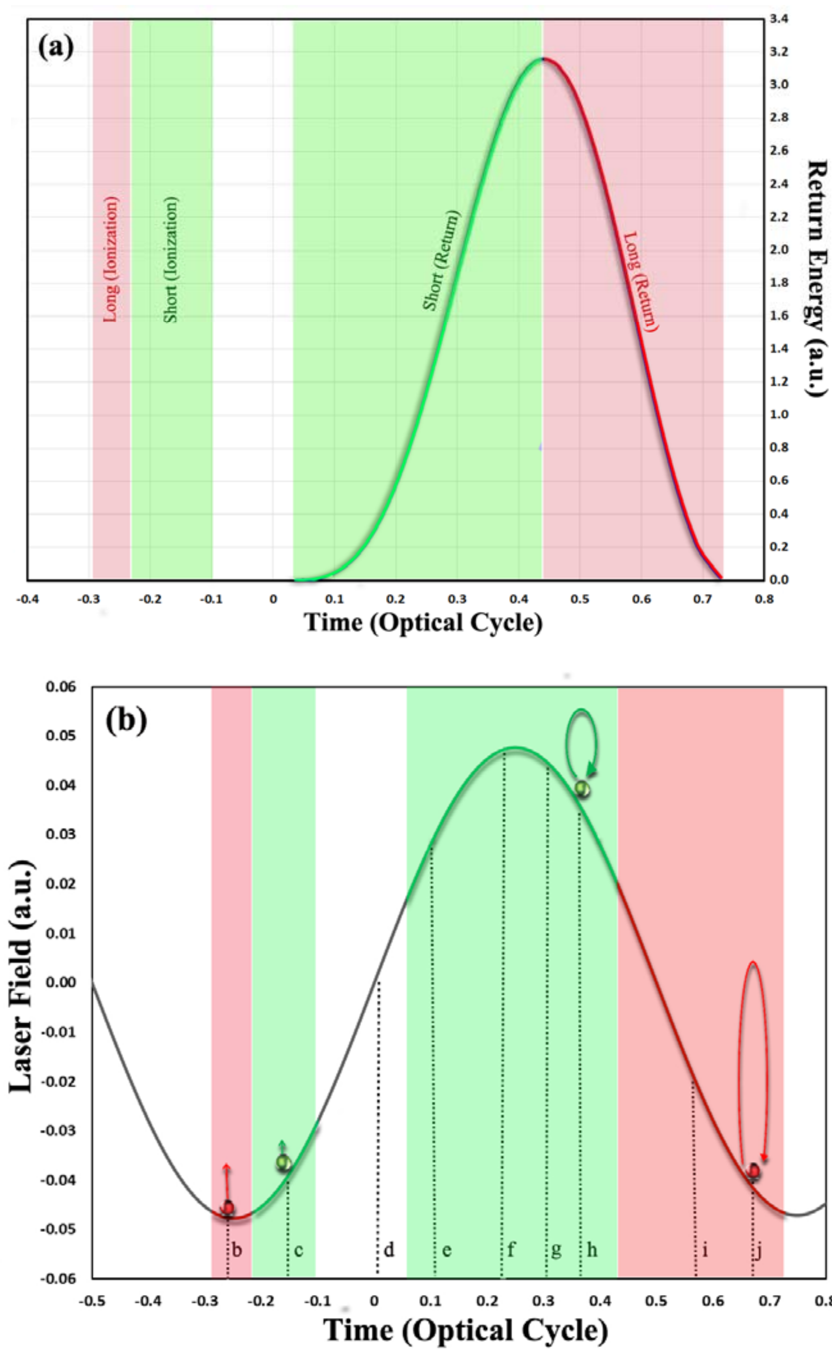

FIG.3. (Color online) (a) Semi-classical return energy as a function of the return time. The red and green lines indicate the long and short trajectories, respectively. (b) Driving laser pulse. Red and green shaded areas correspond to the long and short electron return times. The red and green dots represent samples for each set of trajectories. The curved red and green arrows illustrate, schematically, the long and short and long trajectories. The labels b through j correspond to the time moments for which the electron densities are presented in Fig.2.

Fig. 4(a) shows the wave packets detached from the hydrogen atom at 0.19 o.c. (with respect to the beginning of the 11^{th} o.c.) with different colors. In general, there is a close resemblance of the trajectory patterns in adjacent optical cycles except at the beginning and the end of the laser pulse where the intensity is very low. In Fig. 4(b), we report the corresponding groups of the Bohmian trajectory flows with the same color and labels. To generate the results presented in Fig. 4(b), the initial time for RK4 solver in the current case is set to -0.25 o.c. The initial position of the electron is scanned between $z_0 = 1$ and $z_0 = 10$ a.u., with $x_0 = 1$ a.u. Within each half optical cycle, the outermost wave packets continue moving towards larger distances from the core, thus describing ionization. The corresponding trajectories belonging to this group are indicated by the label “5”. Please note that the ionization probability at the end of the laser pulse, calculated according to Eq. (5), is about 1.4 percent only. The wave packets (and the corresponding trajectories) labeled by “4” and “3” are the ones that oscillate in the external field before leaving the area shown in Fig. 4, without returning close to the core. Labels “2” and “1” indicate some longer and shorter trajectories, respectively. These trajectories represent the travelling wave packets in Fig. 2, which are shaded with the same colors. As can be seen in Fig. 4(b), the longer trajectory “2” reaches its maximum distance (around $z = -30\,a.u.$) at about 0.25 o.c. After this point it travels back and returns to the core at about 0.68 o.c. The shorter (green) trajectory “1”, on the other hand, travels in z-direction to about -15 a.u and then returns back to the target at about 0.37 o.c. (see Fig. 2(h)). This group of trajectories represents the motion of the green shaded wave packet in Fig. 2(d-h). In Fig. 4(b), one can also see the trajectories featuring two returns to the parent ion (blue line). Finally, the innermost trajectories (intense gray area below $z = -5.0\ a.u.$) have smaller momenta and are mainly governed by the Coulomb potential. These trajectories vibrate in a short distance range around the nucleus and describe the dynamical aspects of lower bound states. These results are in complete agreement with the semi-classical picture presented in Fig. 3(a).

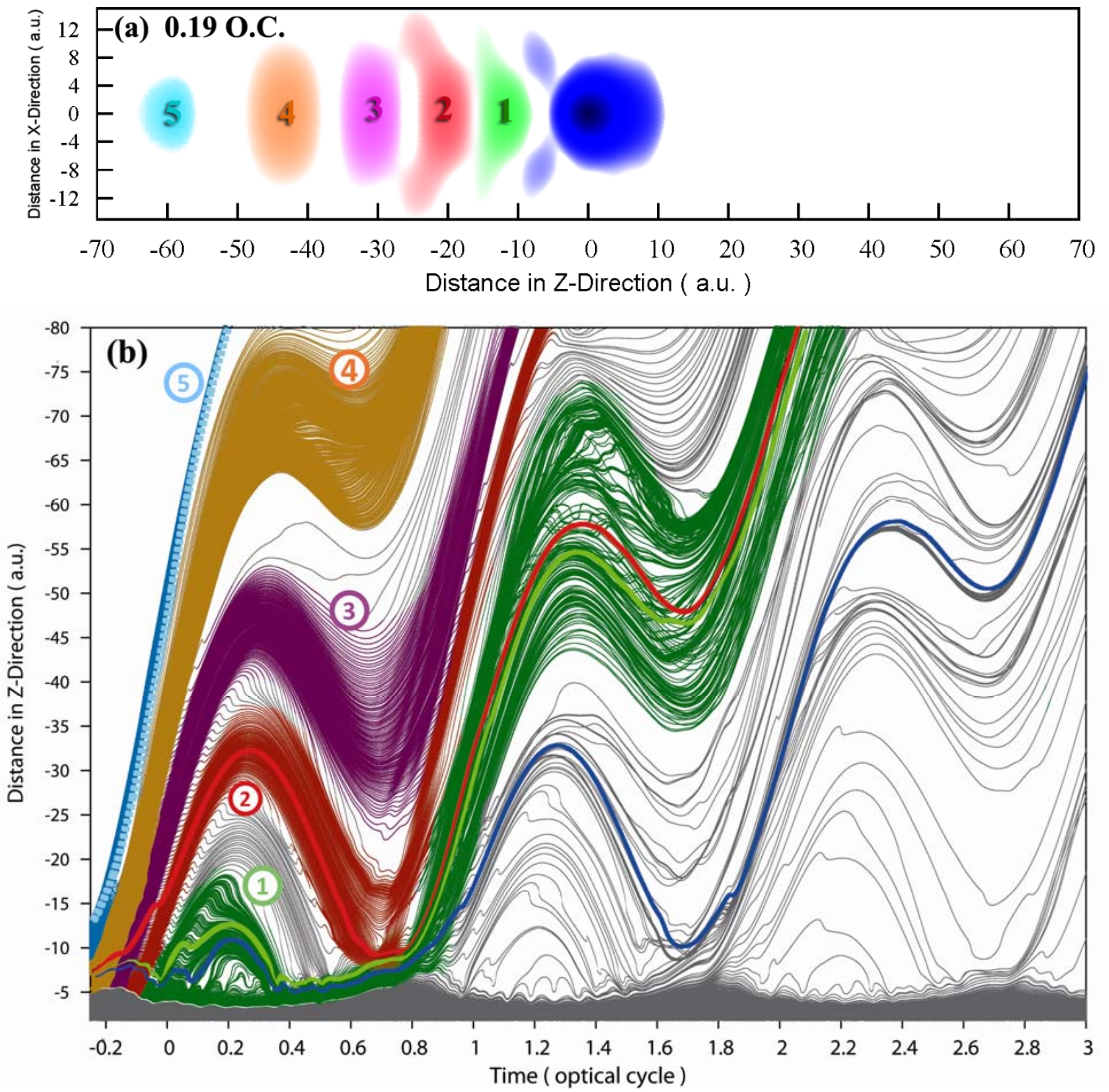

FIG.4. (Color online) (a) Multiple portions of the electron density detached from the hydrogen atom as seen at 0.19 o.c. from the beginning of the 11th o.c. in the sin^2 laser pulse with the carrier wavelength $800\,nm$. Different colors indicate different portions of the electron density (also labeled by "1" to "5"). (b) A thousand of the Bohmian trajectories initiated at $t_0 = -0.25$ o.c. representing the time evolution of the hydrogen atom in the same laser field. The labels "1" and "2" indicate the groups of short and long trajectories, respectively. One trajectory in each group is represented by a bold line. The groups of trajectories labeled by "3" and "4" represent the wave packets that oscillate in the external field without revisiting the core. The trajectories "5" represent the motion of the outermost wave packet. The blue single line shows the trajectory that returns twice to the nucleus. The intense gray area under $z = -5.0\,a.u.$ corresponds to short oscillatory trajectories close to nucleus.

Recently, Telnov *et. al*. reported multiple ionization bursts within a single optical cycle in the time-dependnet ionization rate of the hydrogen atom [8]. The ionization rate is defined by Eqs. (5) and (6) for the whole spherical volume with the radius r_{max} where the time-dependent Schrödinger equation is solved. However, we can also define this rate on the boundary of a smaller spherical volume with the radius $r_c < r_{max}$. Defined in this way, the quantity dP/dt represents the electron current through the sphere of radius r_c. Certainly, this depends on both the time and radius r_c. The time profile of the rate dP/dt changes with the distance r_c [8]. Here we report the sub-cycle structures in the time-dependent rates calculated on the distances as small as few tens of atomic units from the core. We understand that direct measurements of the electron current close to the atomic core could be extremely difficult or even implausible. Experimental observations are more feasible at sufficiently large distances from the target. Of course, in the far asymptotic region, the time-dependent signal would be reshaped due to different times of flight of the electrons with different energies. Still, the information about the sub-cycle structures of the electron current at smaller distances must be encoded in that signal. Then a theoretical procedure can be applied that maps the properties of the outgoing-wave packet at large distances to earlier times and smaller 350 distances. Construction of such a procedure can be a subject of a separate study. In Fig. 5(a) we present the time-dependent ionization rate for the few central optical cycles for $r_c = 25\,a.u.$ One can find in this figure a similar pattern of four bursts at each half optical cycle. The structure of the ionization rate can be explained using the Bohmian trajectories studied here, as well as the electron densities (Fig.2). As it was discussed in [8], the portions of the outgoing wave packet, created under the influence of the external field, contain states belonging to various energies. Different groups of electrons travelling along distinct trajectories can represent this various energy contributions. The Bohmian trajectories in the 11^{th} o.c. optical cycle are shown in Fig. 5(b). As it was mentioned above, the same pattern is observed in other time intervals and the reason for chosing this optical cycle is that the laser intensity is around its maximum. In Fig. 5(b) four groups of trajectories are shaded with different colors (labeled A to D). These groups are responsible for the bursts observed in the ionization rate. Apparently, the intensity of each peak in the ionization rate is related to the number of the Bohmian trajectories found in the corresponding group. Peak A corresponds to the trajectories that represent the first (small) wave packet that does not came back to the core. The next peak (B) corresponds to a more distributed wave packet, which oscillates at a large distance from the core before it eventually leaves the parent ion. The next group of trajectories represents the wave packets created at smaller distances from the nucleus. As one can see in Fig. 4(b), the trajectories C and D can come back closer to the core before they go to large distances describing ionization. Shorter (green) trajectories never reach to -25 a.u., and therefore do not contribute to the ionization rate. Analysis of the Bohmian trajectories, as one can see, provides a simple and intuitive explanation of such a subtle phenomenon as multiple bursts in the time-dependent ionization rate.

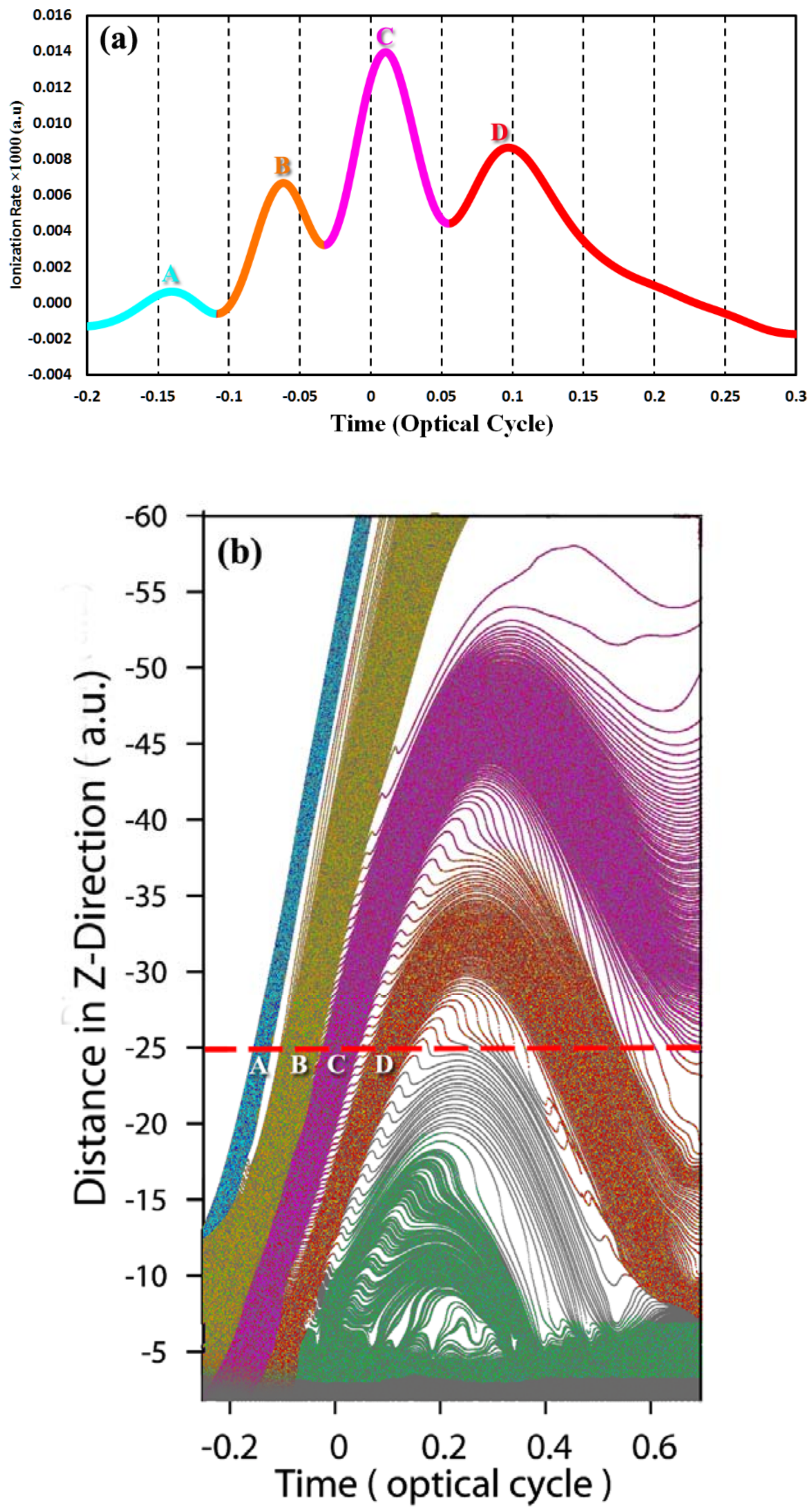

FIG.5. (Color online) (a) Time-dependent ionization rate of the hydrogen atom within a half optical cycle. (b) Four distinct groups of the Bohmian trajectories (labeled A through D), within a half optical cycle, shaded with different colors corresponding to the peaks in the time-dependent ionization rate. The red dashed line shows $r_c = 25 a.u.$

In summary, we presented a fully *ab initio* 3D and accurate treatment of the Bohmian trajectories beyond SFA, and used it to illustrate the formation of sub-cycle transient structures seen in the MPI processes. Electron wave packet dynamics and ionization process on a sub-femtosecond time scale for the hydrogen atom subject to intense near-infrared laser fields were analyzed. As a complementary tool, an accurate treatment of the electron dynamics in the De Broglie–Bohm's framework of the Bohmian mechanics was introduced to investigate the multiple peaks structure of the time-dependent ionization rate within a half optical cycle. The nature of this phenomenon was revealed by the analysis of the time-dependent electron density and the Bohmian trajectories representing different groups of electrons with various ionization times and pathways. The external field causes transitions to the excited bound and continuum states of the unperturbed atom in the course of time, resulting in the oscillations of the electron density. A nonlinear response of the electron density to the laser field through transitions to the excited states leads to shaping of multiple density portions detached from the core during each optical cycle. In the Bohmian trajectory analysis, it is reflected in formation of distinct groups of the trajectories describing ionization. This is the origin of multiple ionization bursts per optical cycle. We have also performed semi-classical simulations, which illustrate various energy contributions to the wave packet created under the influence of the external laser field.

This work was partially supported by the Chemical Sciences, Geosciences and Biosciences Division of the Office of Basic Energy Sciences, Office of Sciences, U.S. Department of Energy. We also acknowledge partial support from the Ministry of Science and Technology of Taiwan and National Taiwan University (Grants No. 104R104021 and No. ERP-104R8700-2). D.A.T. acknowledges partial support from St. Petersburg State University (Grant No. 11.38.654.2013). P.C.L. acknowledges partial support from National Natural Science Foundation of China (Grants No. 11364039 and No. 11465016), Natural Science Foundation of Gansu Province (Grant No. 1308RJZA195), and Education Department of Gansu Province (Grant No. 2014A-010).

References

[1] F. Krausz and M. Ivanov, Rev. Mod. Phys. **81**, 163 (2009).
[2] P. B. Corkum and F. Krausz, Nature Phys. **3**, 381 (2007).
[3] S. Chen, M. J. Bell, A. R. Beck, H. Mashiko, M. Wu, A. N. Pfeiffer, M. B. Gaarde, D. M. Neumark, S. R. Leone, and K. J. Schafer, Phys. Rev. A **86**, 063408 (2012).
[4] M. J. Bell, A. R. Beck, H. Mashiko, D. M. Neumark, and S. R. Leone, J. Mod. Opt. **60**, 1506 (2013)
[5] M. Chini, X. Wang, Y. Cheng, Y. Wu, D. Zhao, D. A. Telnov, S. I. Chu, and Z. Chang, Sci. Rep. **3**, 1105 (2013).
[6] J. Heslar, D. A. Telnov, and S. I. Chu, Phys. Rev. A **89**, 052517 (2014).
[7] K. N. Avanaki, D. A. Telnov, and S.I Chu, Phys. Rev. A **90**, 033425 (2014).
[8] D.A. Telnov, K.N. Avanaki, and S.I. Chu, Phys. Rev. A **90**, 043404 (2014).
[9] N. Takemoto and A. Becker, Phys. Rev. Lett. **105**, 203004 (2010).

[10] P. B. Corkum, Phys. Rev. Lett. **71**, 1994 (1993).
[11] K. C. Kulander, K. J. Schafer, and J. L. Krause, Proceedings of the Workshop on Super-Intense Laser Atom Physics (SILAP) III, edited by P. Piraux (Plenum Press, New York) **316**, 95(1993).
[12] M. Lewenstein, P. Salieres, and A. L'Huillier, Phys. Rev. A **52**, 4747 (1995).
[13] D. Bohm, Phys. Rev. **85**, 166 (1952).
[14] F. S. Mayor, A. Askar, and H. Rabitz, J. Chem. Phys. **111**, 2423 (1999).
[15] C. L. Lopreore and R. E. Wyatt, Phys. Rev. Lett. **82**, 5190 (1999).
[16] R. Guantes, A. Sanz, J. Margalef-Roig, and S. Miret-Artes, Surf. Sci. Rep. **53**, 199 (2004).
[17] J. Wu, B. B. Augstein, and C. F. d. M. Faria, Phys. Rev. A **88**, 023415 (2013).
[18] P. Botheron and B. Pons, Phys. Rev. A **82**, 021404 (R) (2010).
[19] R. Sawada, T. Sato, and K. L. Ishikawa, Phys. Rev. A **90**, 023404 (2014).
[20] J. Wu, B. B. Augstein, and C. F. de Morisson Faria, Phys. Rev. A **88**, 063416 (2013).
[21] S. S. Wei, S. Y. Li, F. M. Guo, Y. J. Yang, and B. Wang, Phys. Rev. A **87**, 063418 (2013).
[22] J. Stenson, and A. Stetz, Eur. J. Phys. **34**, 1199 (2013).
[23] N. Takemoto, and A. Becker, J. Chem. Phys. **134**, 074309 (2011).
[24] S. Dey, and A. Fring, Phys. Rev. A **88**, 022116 (2013).
[25] Y. Song, F. M. Guo, S. Y. Li, J. G. Chen, S. L. Zeng, and Y. J. Yang, Phys. Rev. A **86**, 033424 (2012).
[26] X. M. Tong, and S. I. Chu, Chem. Phys. **217**, 119 (1997).
[27] D. A. Telnov and S. I. Chu, Phys. Rev. A **59**, 2864 (1999).
[28] D. A. Telnov and S. I. Chu, Phys. Rev. A **76**, 043412 (2007).
[29] D. A. Telnov and S. I. Chu, Phys. Rev. A **79**, 043421 (2009).